Performance Evaluation of the Detector and Ultra-Light Micro-cable Assembly for Tracking Application in CBM experiment

Weronika Zubrzycka, Krzysztof Kasiński
zubrzycka@agh.edu.pl, kasinski@agh.edu.pl

Microelectronics Team
Department of Measurement and Electronics
AGH University of Science and Technology,
Av. Mickiewicza 30, 30-059 Cracow, Poland

31.05.2017

Agenda

1. Introduction to CBM experiment and STS detector architecture.
2. Motivation.
3. Sensor and cable models and parameters.
4. The transfer characteristics of the cables and sensors with different load.
5. Studies of the output current pulse shape.
6. Estimation of noise and charge transfer effectiveness.
7. Conclusions

The CBM experiment at GSI

Aim: Creation of the highest baryon densities in nucleus-nucleus collisions, exploration of the properties of the super-dense nuclear matter.

STS (*Silicon Tracking System*) detector

- tracking and momentum determination of the charged particles at the interaction rate of 10 MHz
- 8 tracking stations in distances from 30 cm to 100 cm from the target within a 1T magnetic dipole field

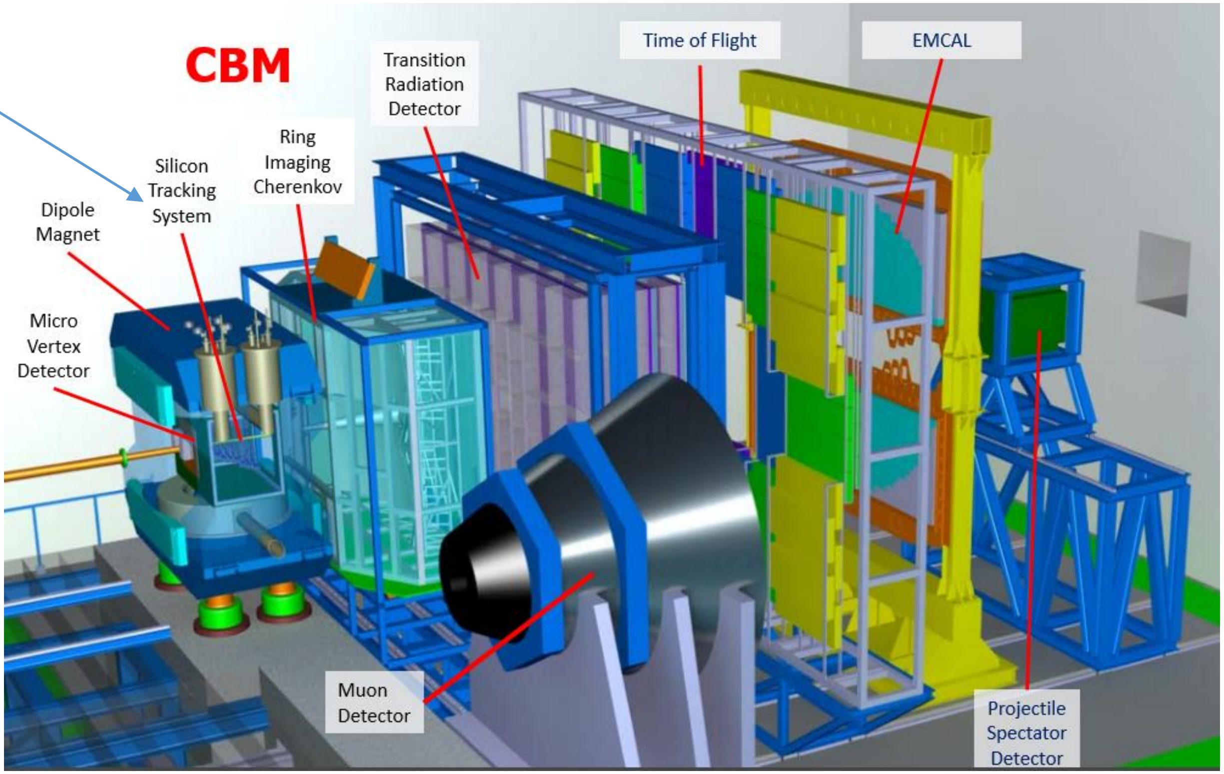

STS metrics:
>1 790 000 channels
>14 000 ASICs
1752 FEBs
600 ROBs
78 DPB s

The CBM experiment at GSI:STS (*Silicon Tracking System*) detector

quarter of a detector station

readout electronics (STS-XYTER2 chips) at the perimeter of the detector stations on FEB boards (8 chips/board) + data concentrators (GBTx-based ROB boards)

multi-line micro-cables -> sensors read out

double–sided, micro-strip sensors, 1024 CH/side, 7.5°stereo angle, 58 μm strip pitch

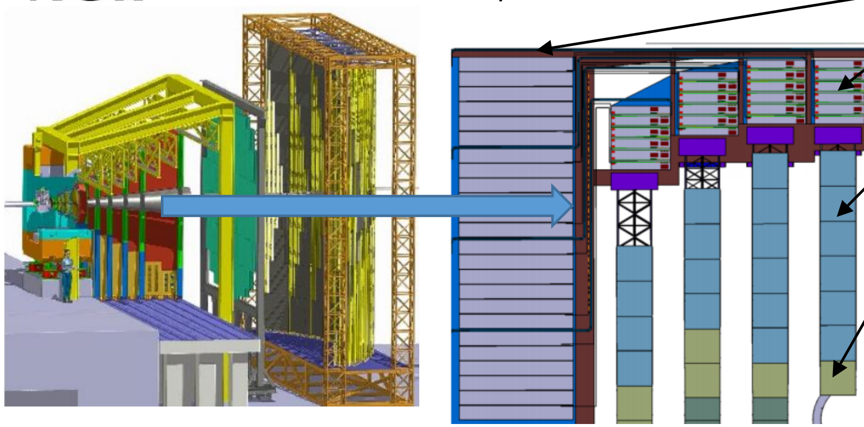

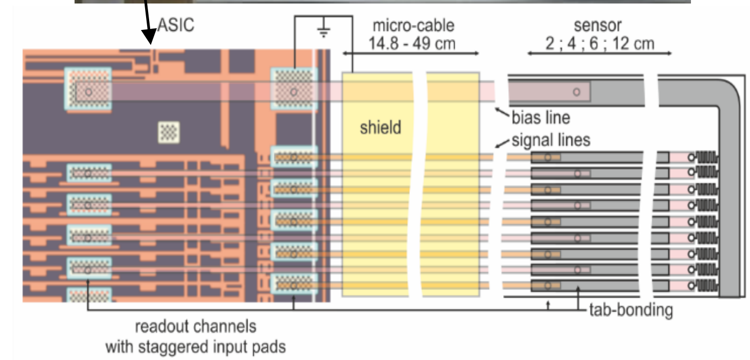

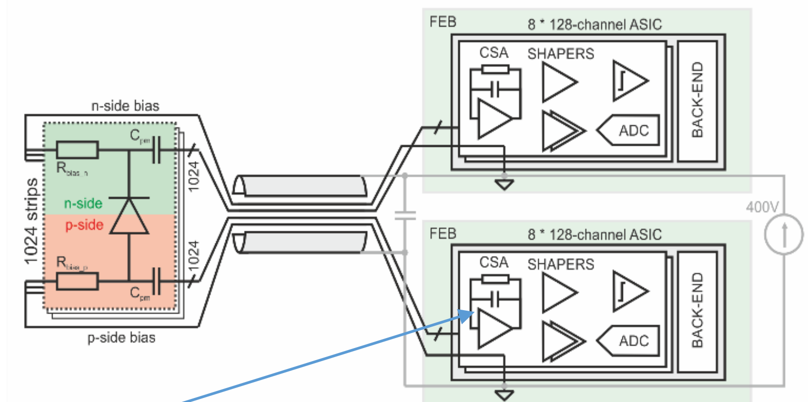

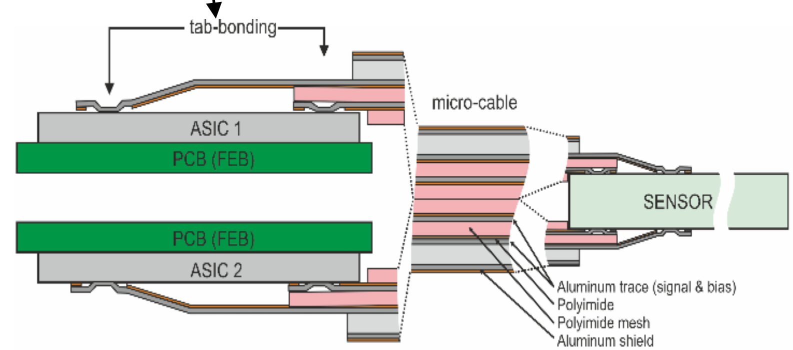

The STS/MUCH-XYTER2:

- developed at AGH University Cracow
- 10 mm × 6.75 mm
- 128 readout channels
- two test channels
- Each channel:
  - Charge Sensitive Amplifier (CSA),
  - Polarity Selection Circuit (PSC),
- fast and a slow pulse shaping amplifiers (shapers),
- timing discriminator
- 5-bit continuous-time, flash analog-to-digital converter (ADC)

Motivation

- **The noise performance of the entire detector module depends on:**
  - the read-out IC architecture and characteristics,
  - power supply system performance,
  - the sensor's and cable's parameters
    - Sensors’ and cables’ capacitance
    - Series resistance of long sensors and cables.
- **Continuously evolving development of the STS detector components required new studies of achievable noise performance in the STS detector system.**

$$\frac{<dv_{CSAout}{}^2>}{df} = \frac{a}{(2\pi f C_{fb})^2} + (b + \frac{A_F}{f})(\frac{C_{tot}+C_{fb}}{C_{fb}})^2$$

$$a = 2qI_{leak} + \frac{4kT}{R_{bias}} + \frac{4kT}{R_f} - \text{current noise},$$

$\text{k} - \text{Boltzmann constant, T} - \text{temperature}$

b – thermal noise of the CSA input transistor

$\frac{A_F}{f}$ - flicker noise of the CSA input transistor

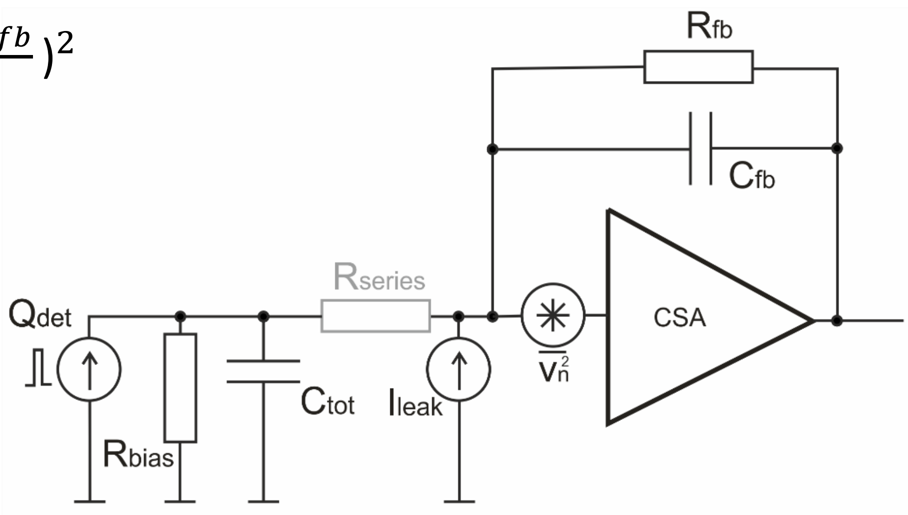

Sensor and cable models

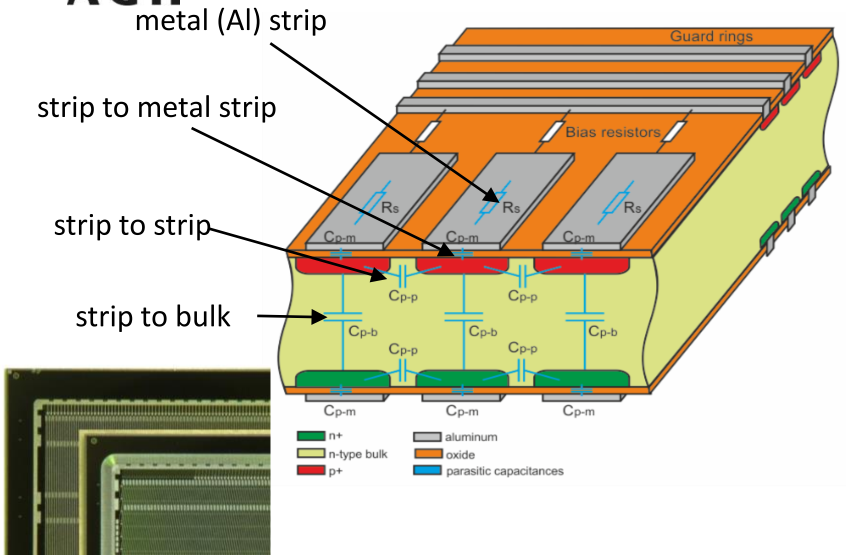

Cross section and parasitic capacitances of double-sided detector

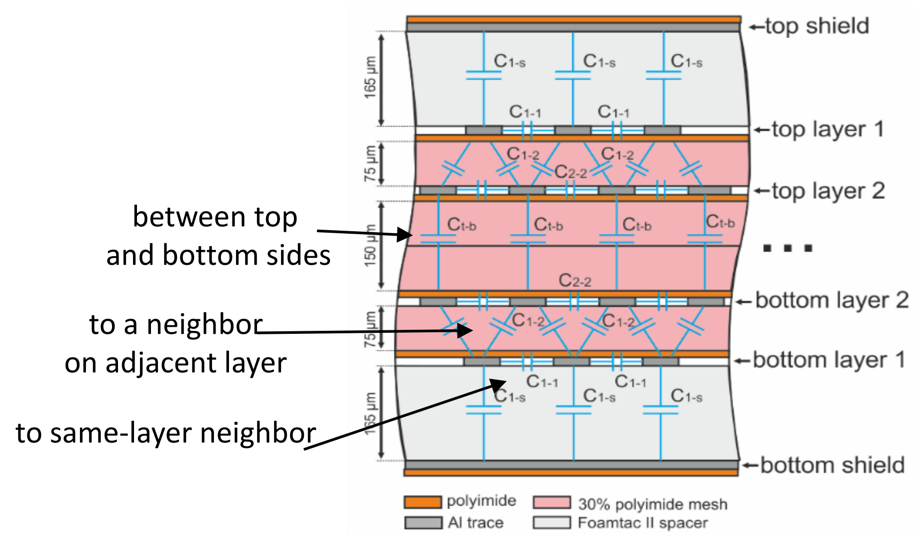

Cross section and parasitic capacitances of ultra-light micro-cable assembly

- array of strip-shaped, reverse-biased diodes on a common bulk;
- 1024 strips with 58 µm pitch;
- 7.5º stereo angle on each side;
- thickness - 300 μm;
- lengths - 2, 4, 6 and 12 cm;
- AC coupled (the coupling capacitor formed with the metal strip deposited over a diffusion strip and an isolation layer);

- multi-line micro-cables;
- 128 thin aluminum trace lines;
- 116 µm pitch, 15 µm thickness, 35 µm width ;
- two polyimide signal layers;
- signals’ transfer between the sensors and front-end (FE) electronics and for the sensors biasing;
- insulating meshed spacer made from polyimide foil between the layers of cables in a bundle -> reduction of the cross-talk and inter-layer capacitance;
- shieliding of the stack with four micro-cable layers (cutting-down the interference coupling).

Sensor and cable models

Sensor parameter	Value FAB1	Value FAB2	Cable parameter	Value
strip to strip C_{p-p} (p+)	0.36 pF/cm	0.43 pF/cm	trace material & dimensions	Al 35 µm × 14 µm
strip to strip C_{p-p} (n+)	0.37 pF/cm	0.57 pF/cm	capacitance to same-layer neighbor $C_{2-2}=C_{1-1}=C_{S-S}$	0.119 pF/cm
strip to metal strip C_{p-m}	10 pF/cm	18 pF/cm	capacitance to a neighbor on adjacent layer C_{1-2}	0.139 pF/cm
strip to bulk C_{p-b}	0.18 pF/cm	0.21 pF/cm	to ground plane C_{2-G}	0.38 pF/cm
metal (Al) strip R_{sm}	10.5 Ω/cm	10.5 Ω/cm	to ground plane C_{1-G}	0.29 pF/cm
strip $R_{sp\ (p+)}$	66 kΩ/cm	66 kΩ/cm	trace series resistance R_s (signal)	0.635 Ω/cm
strip $R_{sp\ (n+)}$	44 kΩ/cm	44 kΩ/cm	trace series resistance R_s (bias)	0.618 Ω/cm
Bias resistance $R_{bias\ (p\text{-}side)}$	500 kΩ/strip	450 kΩ/strip		
Bias resistance $R_{bias\ (n\text{-}side)}$	500 kΩ/strip	1700 kΩ/strip		
Sensor thickness	285 µm	320 µm		
Total strip capacitance				
p-side	1.02 pF/cm	1.74 pF/cm	**Total cable capacitance**	0.382 pF/cm
n-side	1.02 pF/cm	1.52 pF/cm		

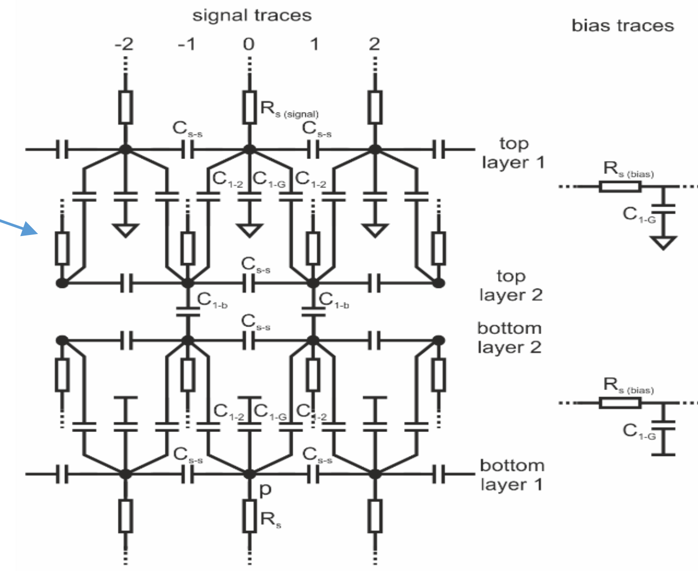

Electrical model of ultra-light micro-cable signal traces and sensor biasing traces

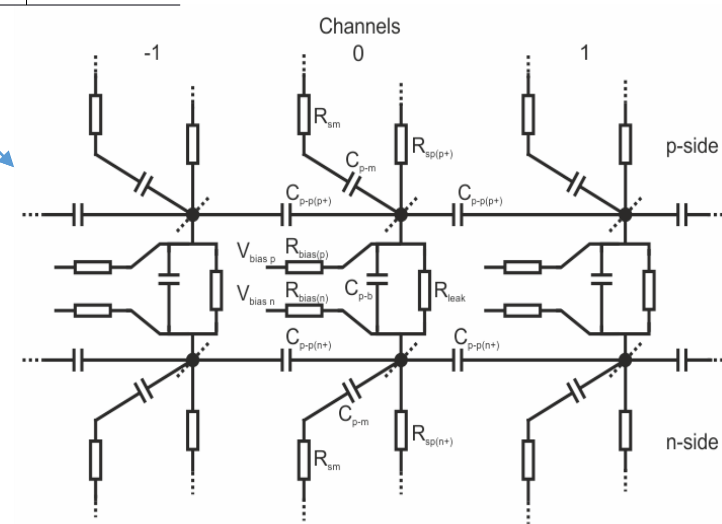

Electrical model of double-sided sensor

Transfer function

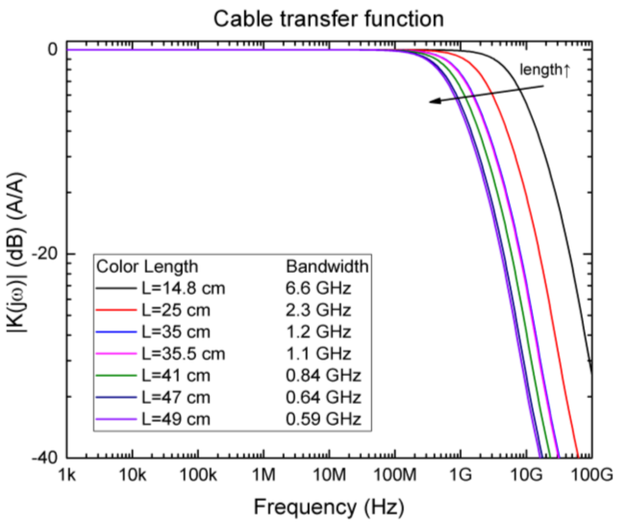

- cable length from 14.8 cm through 49 cm
- ideal load (Zin=0Ω)

- Bandwidth↓ with the increasing length of the cable;
- Bandwith: 0.59 GHz (L=49 cm) to 6.6 GHz (L=14.8 cm).

- sensor's length - 6 cm
- different sides (p or n)
- two vendors
- different parasitic components depending on the side (p or n) and on the manufacturer

bias resistor value (3x higher value for n-side)

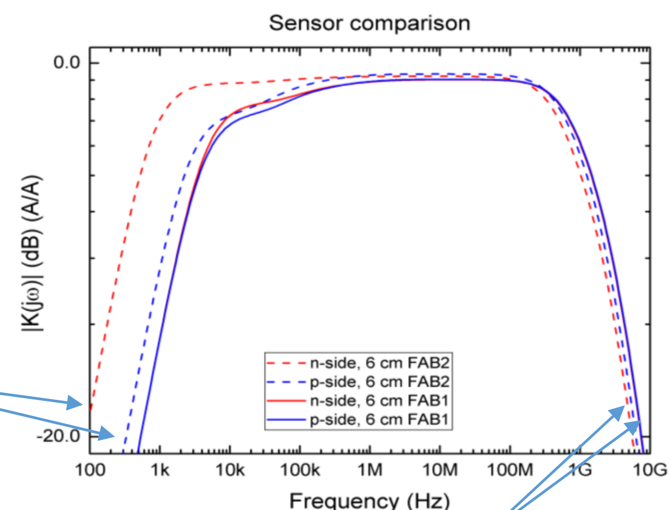

FAB1 - differencies are negligible (<3%).

strip-to-strip capacitance differences between p and n side (31%)

Sensors comparison

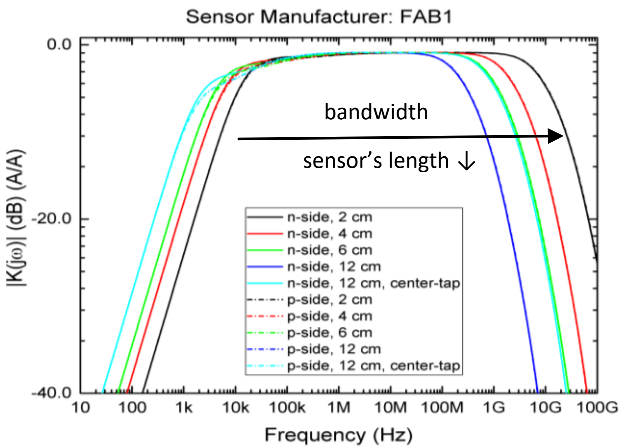

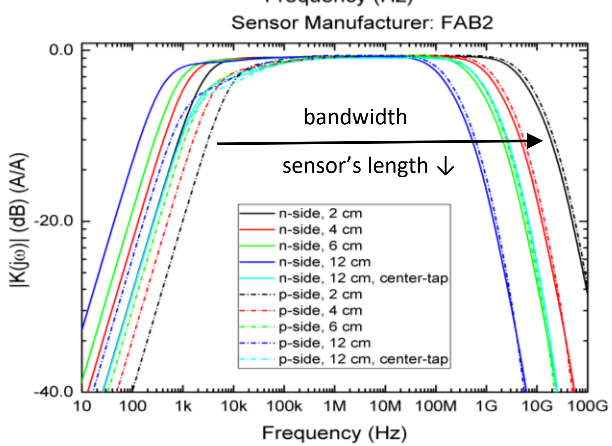

sensors of different lengths from 2 to 12 cm from the two manufacturers

Two sets of cable-sensor lengths, two different manufacturers and for two sides of the sensor, loaded with an ideal amplifier with zero input impedance

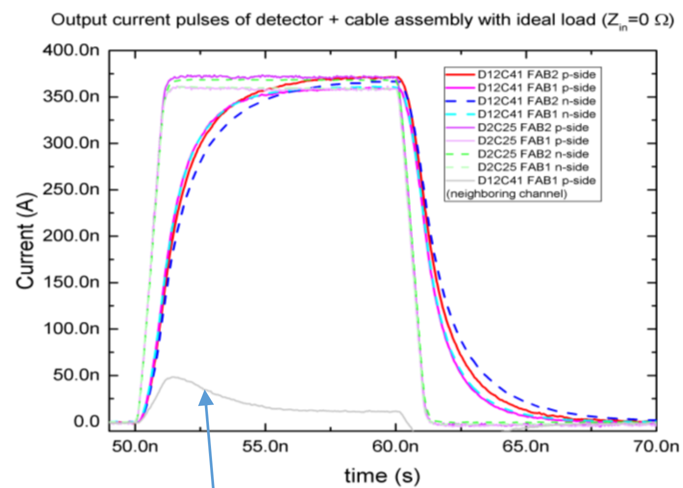

charge leakage to the neighbouring channel

Output current pulse shape simulations

Simulations for three various types of load impedances:

- simple 200 Ω resistor
- simplified CSA model
- fully-featured analog front-end channel implemented in the STS/MUCH-XYTER2 ASIC.

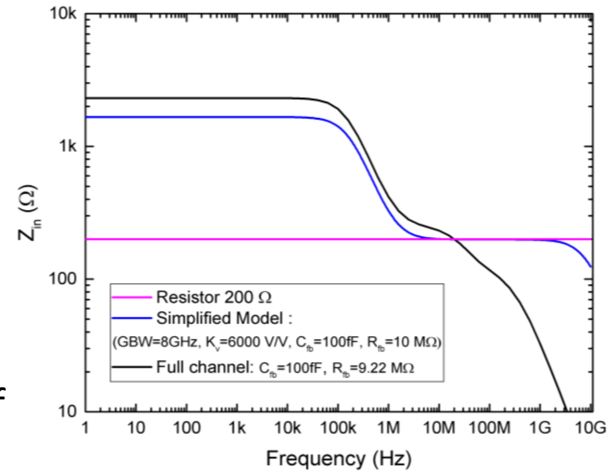

simplified CSA model

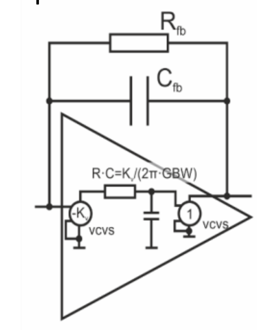

- Charge generated by the ideal current pulse (1 ns rise/fall times, 10 ns width) at the furthest part of the sensor
- The impact of the growing sensor's and cable's lengths on the output pulse shape (amplitude↓, pulse duration↑)

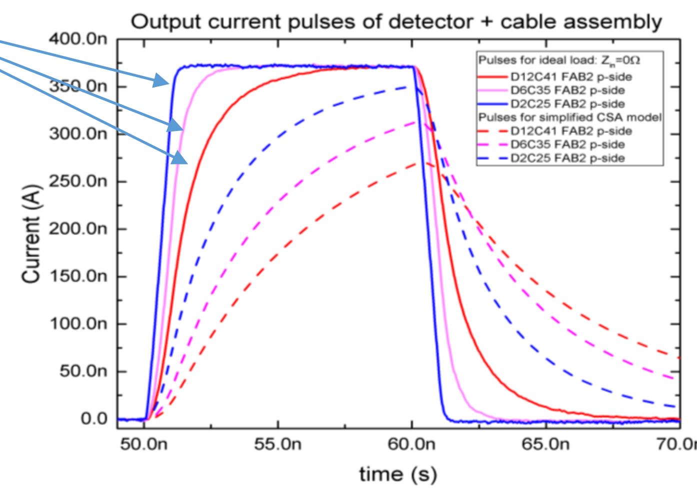

Comparison of ideal load (Z_{in}=0 Ω) and simplified CSA model

The total integrated charge does not change significantly!

Detector / Cable length case	Charge transfer efficiency (source to middle channel) % for ideal load (Z_{in}=0 Ω) % for simplified CSA model % for fully featured channel (I_{leak}=0, no ESD)			
	p-side		n-side	
	FAB1	FAB2	FAB1	FAB2
D: 2 cm C: 25 cm	86.0 % 86.6 % 83.7%	89.8 % 88.9 % 87.4%	88.4 % 86.8 % 84.5%	91.8 % 90.1 % 89.3%
D: 6 cm C: 35 cm	87.4 % 86.8 % 84.0%	90.4 % 88.9 % 87.5%	89.3 % 86.7 % 84.5%	92.1 % 89.8 % 88.2%
D: 12 cm C: 41 cm	88.3 % 86.6 % 85.7%	91.4 % 90.0 % 88.1%	90.31 % 86.6 % 86.0%	92.2 % 90.1 % 87.1%

Noise simulations' results

- The sets of the sensor from two considered manufacturers,
- Sensors: length from 20 mm up to 120 mm
- Cables:length from 148 mm to 490 mm

- measured channel of the STS/MUCH-XYTER2 loaded with full analog charge processing chain,
- the neighboring channels were loaded with 200 Ω resistors

Summary of the ENC values obtained for selected cases

Sensor length: D Cable length: C		ENC (e^- rms) @ I_d=2mA, t_p=150 ns, R_f=9.22 MΩ (% charge transferred to the FE channel)			
		I_{leak}=0, no ESD circuit	I_{leak}=0, with ESD circuit	I_{leak}=8nA/cm, with ESD circuit	I_{leak}= 400 nA/sensor, with ESD circuit
D: 6 cm C: 14.8 cm FAB1/FAB2	e^+	466.5 / 399.4 (85.4% / 88.9%)	479.1 / 411.5 (85.4% / 88.9%)	535.5 / 478.9 (84.9% / 88.6%)	825.2 / 808.6 (81.7% / 86.4 %)
	e^-	545.2 / 485.4 (85.7% / 89.5%)	559.2 / 498.3 (85.7% / 89.4%)	613.8 / 562.6 (85.3% / 89.1%)	903.4 / 893.3 (82.1% / 87.0%)
D: 2 cm C: 25 cm FAB1/FAB2	e^+	470 / 388.9 (83.7% / 87.4%)	482.7 / 400.8 (83.7% / 87.3%)	501.5 / 424.9 (83.3% / 87.1%)	776.3 / 779.8 (74.5% / 81.4 %)
	e^-	548.5 / 476.3 (84.5% / 89.3%)	562.7 / 489 (84.5% / 89.3%)	580.7 / 511.5 (84.1% / 89.1%)	850.5 / 864 (75.3% / 83.4%)
D: 6 cm C: 35 cm FAB1/FAB2	e^+	530 / 481.6 (84.0% / 87.5%)	543.9 / 495.1 (84.0% / 87.5%)	592.9 / 550.9 (83.6% / 87.2%)	857.4 / 846.6 (80.5% / 85.1%)
	e^-	606.1 / 563 (84.5% / 88.2%)	621.9 / 577.9 (84.5% / 88.2%)	670 / 632.5 (84.1% / 87.9%)	935.8 / 931.6 (81.0% / 85.8%)
D: 2 cm C: 47 cm FAB1/FAB2	e^+	542.5 / 478.8 (82.3% / 85.9%)	556.7 / 492.3 (82.3% / 85.8%)	602.1 / 511.4 (81.1% / 85.6%)	816.2 / 822 (73.4% / 80.1%)
	e^-	618.4 / 561 (83.3% / 88.0%)	634.5 / 575.9 (83.2% / 87.9%)	790.2 / 796.9 (82.9% / 87.7%)	891 / 906.7 (74.3% / 82.2%)
D: 4 cm C: 49 cm FAB1/FAB2	e^+	565.5 / 515.2 (82.7% / 86.3%)	580 / 529.2 (82.7% / 86.3%)	610.4 / 564.2 (82.3% / 86.0%)	866.3 / 858.8 (77.9% / 83.1%)
	e^-	640.8 / 595.8 (83.5% / 87.6%)	657.4 / 611.5 (83.5% / 87.6%)	687.4 / 646.1 (83.1% / 87.3%)	944.2 / 944.5 (78.6% / 84.4%)
D: 12 cm C: 41 cm Centertap FAB1/FAB2	e^+	600.7 / 591.5 (84% / 87%)	615.7 / 606.4 (84.0% / 86.9%)	699.2 / 693.6 (83.5% / 86.6%)	907.3 / 911.2 (82.0% / 85.5%)
	e^-	675.2 / 669.2 (84.4% / 86.9%)	692.5 / 686.4 (84.4% / 86.8%)	775.9 / 774.1 (83.9% / 86.5%)	987.1 / 996.5 (82.3% / 85.4%)
D: 12 cm C: 35.5 cm Endtap FAB1/FAB2	e^+	590 / 590.4 (84.4% / 87.3%)	604.8 / 605.2 (84.3% / 87.3%)	690.2 / 693.2 (83.8% / 86.9%)	903.1 / 913.4 (82.2% / 85.8%)
	e^-	664.8 / 668.3 (84.7% / 87.2%)	681.8 / 685.3 (84.7% / 87.2%)	767.1 / 773.8 (84.2% / 86.8%)	983.1 / 999.1 (82.6% / 85.6%)

- lower noise levels -> FAB2 sensors,
- ENC values for freshly fabricated sensors: **425 - 797 e- rms,**
- this result will be significantly affected by the increased leakage current due to the aggregated TID (**780 – 1016 e- rms),**
- the **end-tapped** long sensor appears to perform better compared to the center-tapped one.

noiseless power supplies, interferences that may occur in the assembled system not considered in simulations

Contribution of the biasing resistor noise

Conclusions:CiS behave better although the parasitic capacitance is larger!
This is due to the biasing resistor thermal noise -> larger biasing resistance results in lower overall noise.

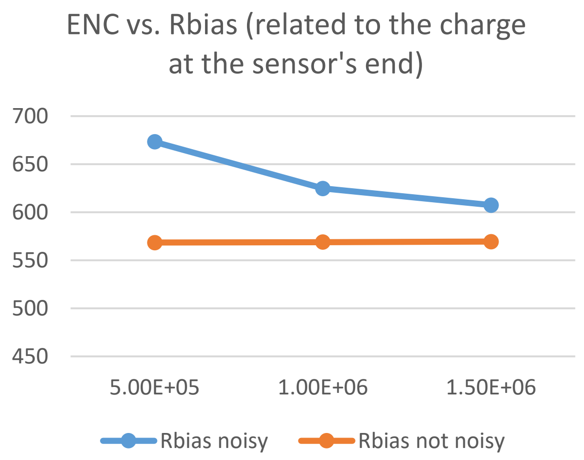

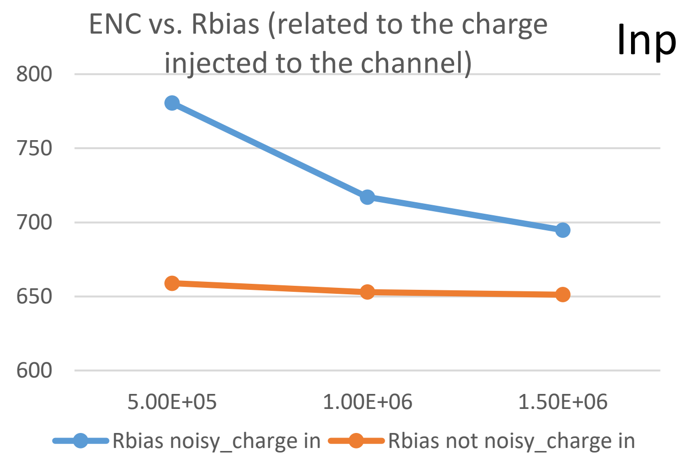

Input charge: 4 fC

1) Case for the biasing resistor generating noise; 2) Biasing resistor is noiseless

Sensor: Hamamatsu, 12cm, n-side (electrons), without cable. Lekagae current I_{leak}= 8nA/cm.

The noise introduced by Rbias (n-side) related to the overall noise is ~17% (based on simulated list of noise contributors).

Conclusions

1. The overall noise level of the entire system depends on the processing chain performance and sensor's / cable's length in conjunction with load impedance characteristics.

2. The comparison of the charge transfer effectivness and noise performance of the sensors with different lengths provided by two differen manufacturers will be important issue in the CBM experiment construction.

3. The ENC value versus biasing resistance considerations will be helpful in sensors' selection for the target aplication.

4. Obtained noise levels show that the architecture and design variables settled in recently fabricated prototype samples can be considered as the ones desired for mass production.

References

[1] Heuser, J., "The Compressed Baryonic Matter Experiment at FAIR," Nucl. Phys. A 904-905, 941c-944c (2013).

[2] Heuser, J., Müller, W., Pugatch, V., Senger, P. , Schmidt, C.J. , Sturm, C. , Frankenfeld, U. , eds., "GSI Report 2013-4] Technical Design Report for the CBM Silicon Tracking System (STS)", GSI, Darmstadt, 2013. http://repository.gsi.de/record/54798.

[3] Kasinski, K., Kleczek, R. and Szczygiel, R., "Front-end readout electronics considerations for Silicon Tracking System and Muon Chamber," J. Instrum. 11, (2016). doi:10.1088/1748-0221/11/02/C02024.

[4] Kasinski, K., Kleczek, R., "A flexible, low-noise charge-sensitive amplifier for particle tracking application", 2016 Mix. - 23rd Int. Conf. Mix. Des. Integr. Circuits Syst., 2016: pp. 124–129. doi:10.1109/MIXDES.2016.7529715.

[5] Otfinowski, P., Grybos, P., Szczygiel, R., Kasinski, K., "Offset correction system for 128-channel self-triggering readout chip with in-channel 5-bit energy measurement functionality," Nuclear Instruments and Methods in Physics Research, Section A 780, 114-118 (2015).

[6] Kasinski, K. , Szczygiel, R. , Zabolotny, W. , Lehnert, J. , Schmidt, C.J. , Müller, W.F.J. , "A protocol for hit and control synchronous transfer for the front-end electronics at the CBM experiment", Nucl. Instruments Methods Phys. Res. Sect. A Accel. Spectrometers, Detect. Assoc. Equip. 835 (2016) 66–73. doi:http://dx.doi.org/10.1016/j.nima.2016.08.005.

[7] Lehnert, J. , Byszuk, A.P. , Emschermann, D., Kasinski, K. , Müller, W.F.J. , Schmidt, C.J., Szczygiel, R. , Zabolotny, W.M. , "GBT based readout in the CBM experiment", J. Instrum. 12 (2017) C02061. http://stacks.iop.org/1748-0221/12/i=02/a=C02061.

[8] Kasinski, K. , Szczygiel, R. , Zabolotny, W. , "Back-end and interface implementation of the STS-XYTER2 prototype ASIC for the CBM experiment", J. Instrum. 11 (2016) C11018. http://stacks.iop.org/1748-0221/11/i=11/a=C11018.

[9] Grybos, P., "Front-end Electronics for Multichannel Semiconductor Detector Systems", Warsaw: Institute of Electronic Systems Warsaw University of Technology, 132-135 (2010).

[10] Kipnis, I., „Noise due to Strip Resistance in the ATLAS SCT Silicon Strip Module", Lawrence Berkeley National Laboratory (1996).

[11] Barichello G. et al. "Performance of long module of silicon microstrip detector", Nucl. Instr. And Meth. A 413 17-30 (1998).

[12] Kasiński, K., Szczygieł, R., "Wpływ szeregowej rezystancji przewodów oraz półprzewodnikowych detektorów paskowych na parametry szumowe układu detekcyjnego", Elektron. Konstr. Technol. Zastos. Vol. 53, nr 3 (2012) 61–64.